Force Prediction Using Fingernail Imaging: An Overview

Tom Grieve, Yu Sun, John M. Hollerbach, and Stephen A. Mascaro

University of Utah, Salt Lake City, UT 84112, U.S.A.
University of South Florida, Tampa, FL 33620-5399, U.S.A.
tom.grieve@utah.edu, yusun@cse.usf.edu,
jmh@cs.utah.edu, smascaro@mech.utah.edu

Abstract. This paper presents a method for automatically calibrating a fingernail imaging system used to detect arbitrary three-dimensional force on the human fingerpad. The calibration is accomplished using a Magnetic Levitation Haptic Device modified to apply calibrated forces through a flat plate to the fingerpad.

The technique explained here is shown to accurately predict arbitrary shear force with RMS error of 0.3 N (which is 3% of the full range of ± 5 N) and normal force with RMS error of 0.5 N (which is 5% of the full range of $0 - 10$ N). The paper also demonstrates the model and explains some of the methods used to compensate for nonlinearities in the fingernail coloration response.

Keywords: Force sensing, Haptics, Grasping.

1 Introduction

Fingernail imaging as a method for detecting force on the human fingerpad is based on the coloration effect illustrated in Figure 1. As the finger is pressed against a surface, the interactions between the bone and nail compress regions of the finger pulp and thereby constrict blood flow through the capillaries. This causes blood to pool in some regions while evacuating other areas, creating a band near the distal end of the fingernail which begins to whiten. Simultaneously, the rest of the nail except the lunula reddens. Additionally, areas of the flesh alongside the nail whiten. If, in addition to normal force, shear force is applied to the fingerpad, different patterns appear on the nail.

This effect is fast, requiring less than one second to reach steady-state. The coloration response described here is broadly similar in the general population [1] and so studies of this effect are applicable to a wide range of people. Surprisingly, when individual calibration is applied, it is possible not simply to qualitatively predict the direction of the force, but also to quantitatively estimate the magnitude with a reasonable degree of accuracy. This paper presents the current method of calibration for fingernail imaging used to create a model for predicting fingertip force.

Mascaro and Asada [2] first proposed fingernail imaging as a method for detecting force on the human fingerpad. That work used a combination of photodetectors and LEDs embedded in an on-nail sensor to illuminate and perceive the coloration changes. These wearable sensors, with appropriate calibration, were able to predict shear force with an RMS error of 0.5 N over a range of ± 2.25 N and normal force with an RMS

J.A. Cetto et al. (Eds.): Informatics in Control, Automation and Robotics, LNEE 89, pp. 37–48.
springerlink.com

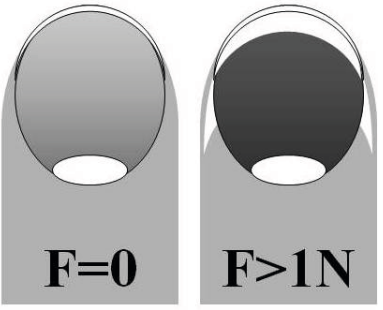

Fig. 1. Illustration of Coloration Effect: (Left) Finger with no Contact (Right) Finger with 1N Normal Contact Force.

error of 1.0 N over a range of $0 - 3$ N [3]. There are, however, two limitations in these sensors. Space restrictions prevent more than a few photodetectors being placed on the nail, which limits the amount of data that may be recorded from the technique. Additionally, the sensors must be custom manufactured for each test subject.

To bypass these restrictions, the development of a high-resolution imaging technique was created [4]. This involves capturing images of the fingernail and the surrounding skin with a digital camera. This method was able to predict normal force with an RMS error of 0.3 N over a range of $0-10$ N. Later experiments improved this prediction error to just 0.1 N when simultaneously predicting normal forces over a range of $0-10$ N and shear forces oriented either laterally (across the finger) or longitudinally (along the finger) over a range of ± 2 N [5]. Another important result of these initial experiments was that the green channel in an RGB image showed the largest response to the force. In addition, it was found that the direction of the force could even be qualitatively estimated without individual calibration with 90% accuracy [6]. These levels of accuracy were found to hold even as the resolution of the images was reduced to 10×10, indicating that extremely high-resolution images were not necessary for accurate measurements. However, this method introduced new challenges, most notably positioning the finger relative to the camera and adjusting for differences in lighting. For the time being, these have been carefully controlled, but they will need to be addressed at a future time.

Both methods have been shown to be accurate in predicting both the magnitude and direction of force, but require individual calibration. The automated calibration technique presented here is able to predict arbitrarily-directed shear force with an RMS error of ± 0.3 N over a range of ± 2.5 N and normal force with an RMS error of ± 0.3 N over a range of $0 - 10$ N [7]. Section 2 of this paper demonstrates the automated calibration procedure. Section 3 contains a discussion of the analysis techniques used on the calibration data. This includes the method used for image registration as well as the model developed to represent the effect of force on the coloration effect. The least-squares method used to generate the values used in the model is discussed. Section 4 presents some results from the model and outlines possibilities for future work.

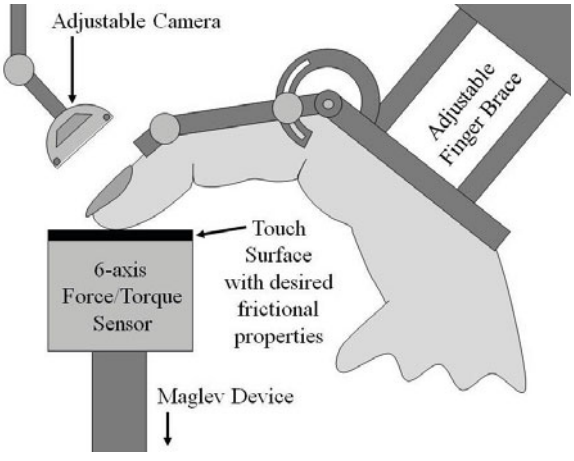

Fig. 2. Diagram of Calibration Setup.

2 Calibration Procedure

To achieve the stated accuracy of force prediction, individual calibration is necessary. This calibration procedure follows a general form: A finger is placed on a force sensor with a camera placed above. A series of forces is exerted between the finger and the sensor while the camera records images. Once the calibration is finished, these images are compared to the data obtained from the force sensor to form a model for prediction. Although in the past, manual calibration has been performed, requiring the test subject to exert forces, the fatigue that resulted limited a 20-minute session to capturing fewer than 100 images. To allow for faster calibration and reduce the fatigue on the test subject, an automated calibration procedure has been developed.

Automated calibration requires a special setup such as that shown in Figure 2. The test subject's finger is placed in a passive restraint that restricts movement and adjusts the finger joint angles without affecting blood flow. The force sensor is attached to a force-controlled Magnetic Levitation Haptic Device (MLHD) [8]. A camera is placed above the finger to record the images. The MLHD applies the desired force to the test subject and records both image and force automatically. The characteristics of the MLHD are such that the calibration routine is capable of recording one image every 0.5 seconds. In a 20-minute session with a few short breaks, more than 1,500 images may be collected. The actual calibration setup is shown in Figure 3.

The MLHD is controlled by means of a standard PIV force feedback controller with a feed-forward term. The signal from the controller is sent to the MLHD as a force command. This controller has a relatively slow step response, with a 98% settling time of 0.2 seconds. Since the calibration trajectories do not use steps in force but ramps, this is not a problem during calibration.

The desired force space to be covered during calibration is a cone with a slope equal to the coefficient of static friction μ between the finger and the contact surface. Different calibration trajectories have been designed to cover the force space in different ways.

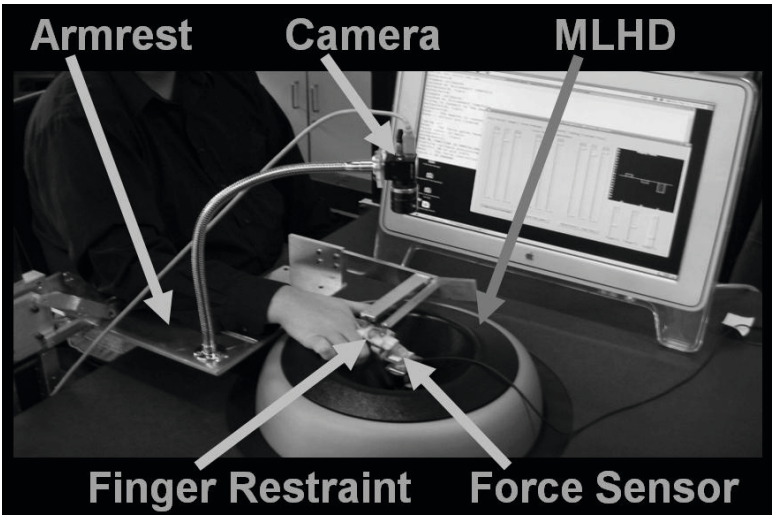

Fig. 3. Photo of Calibration Setup.

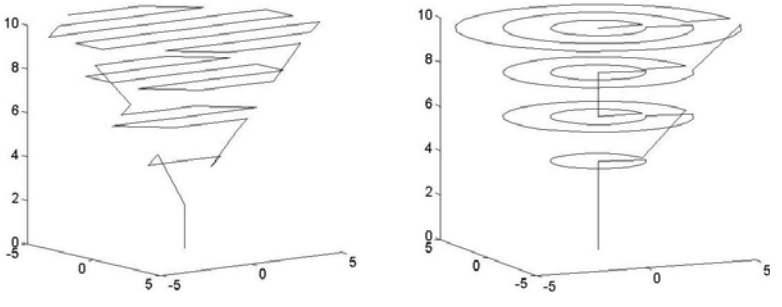

Fig. 4. Example Calibration Trajectories.

Two sample calibration trajectories are shown in Figure 4. Some use a Cartesian (x-y-z) grid, while others use cylindrical coordinates (r-θ-z). The distance between adjacent points on the grid, ΔF varies, as does the value used for μ, the slope of the outside edge of the cone. During calibration, each force level is held for 0.4 seconds to allow the camera time to record an image. Then a 0.1-second ramp is used to transition to the next force level.

3 Data Analysis

Once collected, the calibration data must be processed to develop a model that may then be used to predict force. The processing takes place in two steps: Registration and Model Formulation.

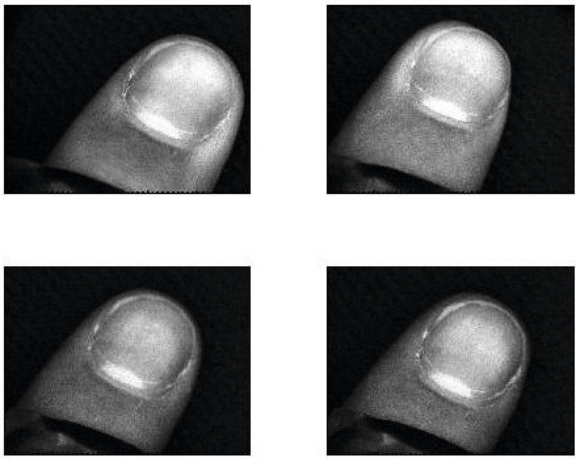

Fig. 5. Finger Images Demonstrating the Need for Registration.

3.1 Registration

The problem of registration is evident in Figure 5. Here, four calibration images are shown. Although the viewing plane of the camera is still parallel to the plane of the fingernail, the position and orientation of the finger has shifted in each of the images. Before these images can be used to generate a model relating pixel intensity to force, they must be registered so that all images have the finger in the same position. One challenge of this task is that the finger is relatively featureless compared to typical registration subjects. Additionally, the calibration itself varies the intensities within the finger, potentially changing some features that might otherwise be used to register the nail.

Although several registration methods have been explored, the current procedure uses what is known as the Scaled Rigid-Body Transformation. This takes advantage of the knowledge that the image plane is always parallel to the finger during calibration. Since the finger only rotates in-plane, it is can be shown that proper registration requires only translations and rotations about the z-axis of the finger. The process is illustrated in Figure 6. An original image is shown in part (a). The finger is found in the image through a connected component analysis and the major axis of the finger is determined (b). This axis is rotated to a predetermined orientation (c) and the image is cropped to include only the largest connected component (d). The image may then be resized as needed to correspond to the target resolution.

3.2 Finger Model

A model of the coloration response of the finger related to force on the fingerpad was first explored in [2]. This initial model was highly nonlinear and took into account the dynamic behavior of the fingernail and surrounding skin. Later experiments [9] have

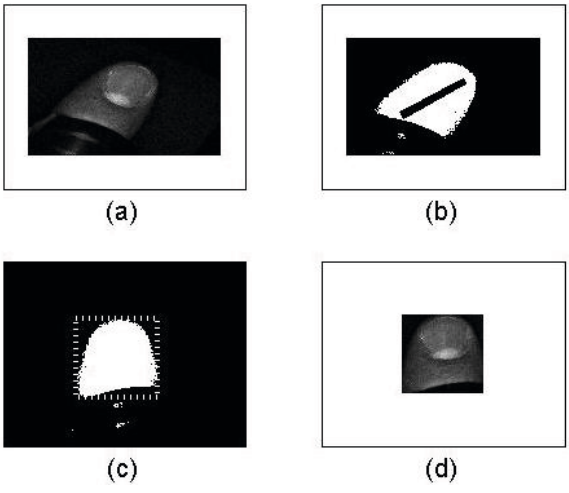

Fig. 6. Registration Procedure (a) Original Image (b) Largest Connected Component with Major Axis (c) Rotated Image with Bounding Box (d) Cropped Image.

shown that the dynamic response of the fingernail is fast enough that it is not necessary for most purposes to account for this, and so the dynamic response is not considered here.

Independence. The static nonlinear behavior of the fingernail may be categorized in one of two general types: independence and saturation. Independence refers to the way that certain regions' coloration response is independent of force in one, two or all three directions of force. For example, the lunula (the light-colored crescent-shaped area at the base of the nail) does not change color in response to any force. Other regions respond only to force in one direction. Research into methods for correcting for this type of nonlinearity is currently ongoing.

Saturation. Certain regions of the fingernail and surrounding skin saturate at relatively low levels of force, while other areas continue to change color even as the normal force exceeds 10 N. When considering only one direction of force, it is relatively easy to see a sigmoid shape appear in the data. As multiple directions of force are added, the response becomes more difficult to visualize and it is more challenging to recognize patterns of saturation.

The procedure to compensate for saturation is illustrated in Figure 7. First, the data is sorted to reveal the saturation. A fourth-order polynomial is fitted to the data. The maximum value of the gradient of that polynomial is found. The data points above and below that maximum value where the gradient reaches 20% of the maximum are found. The intensities of those two points are identified as the upper and lower saturation threshhold, respectively. If no upper or lower saturation limit is found, the minimum or maximum intensity of the pixel is chosen for the respective saturation limit. The data between these two limits is then chosen and fit using the linear model detailed next.

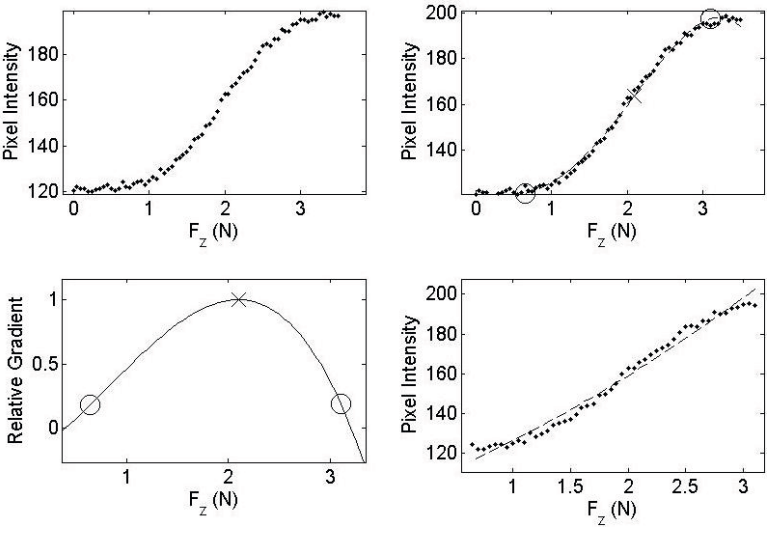

Fig. 7. Saturation Detection in One Force Dimension.

Linear Model. The linear model of the finger is based on the assumption that the intensity of a given pixel (p_i) is a linear combination of the applied forces (f_x, f_y and f_z) with some offset. This results in an equation for the ith pixel:

$$p_i = a_i + b_i f_x + c_i f_y + d_i f_z \tag{1}$$

An $m \times n$ image represented by a pixel vector $\mathbf{p} = \begin{bmatrix} p_1 \; p_2 \cdots p_{mn} \end{bmatrix}^T$ with a corresponding force vector $\mathbf{f} = \begin{bmatrix} f_x \; f_y \; f_z \end{bmatrix}^T$ may then be represented by a single matrix equation:

$$\begin{bmatrix} p_1 \\ p_2 \\ \vdots \\ p_{mn} \end{bmatrix} = \begin{bmatrix} a_1 & b_1 & c_1 & d_1 \\ a_2 & b_2 & c_2 & d_2 \\ \vdots & \vdots & \vdots & \vdots \\ a_{mn} & b_{mn} & c_{mn} & d_{mn} \end{bmatrix} \begin{bmatrix} 1 \\ f_x \\ f_y \\ f_z \end{bmatrix} \tag{2}$$

To form a matrix equation representing an entire calibration set of k images, first the transpose is taken:

$$\begin{bmatrix} p_1 \; p_2 \cdots p_{mn} \end{bmatrix} = \begin{bmatrix} 1 \; f_x \; f_y \; f_z \end{bmatrix} \begin{bmatrix} a_1 \; a_2 \cdots a_{mn} \\ b_1 \; b_2 \cdots b_{mn} \\ c_1 \; c_2 \cdots c_{mn} \\ d_1 \; d_2 \cdots d_{mn} \end{bmatrix} \tag{3}$$

The k equations are then stacked:

$$\begin{bmatrix} {}^1p_1 & {}^1p_2 & \cdots & {}^1p_{mn} \\ {}^2p_1 & {}^2p_2 & \cdots & {}^2p_{mn} \\ \vdots & \vdots & \ddots & \vdots \\ {}^kp_1 & {}^kp_2 & \cdots & {}^kp_{mn} \end{bmatrix} = \begin{bmatrix} 1 & {}^1f_x & {}^1f_y & {}^1f_z \\ 1 & {}^2f_x & {}^2f_y & {}^2f_z \\ \vdots & \vdots & \vdots & \vdots \\ 1 & {}^kf_x & {}^kf_y & {}^kf_z \end{bmatrix} \begin{bmatrix} a_1 & a_2 & \cdots & a_{mn} \\ b_1 & b_2 & \cdots & b_{mn} \\ c_1 & c_2 & \cdots & c_{mn} \\ d_1 & d_2 & \cdots & d_{mn} \end{bmatrix} \tag{4}$$

forming a matrix equation $\mathbf{P} = \mathbf{FA}$. These equations are then solved using standard Ordinary Least Squares (OLS):

$$\mathbf{A} = \left(\mathbf{F}^T\mathbf{F}\right)^{-1}\mathbf{F}^T\mathbf{P} \tag{5}$$

The next section explains how the matrix $\mathbf{A}$ is used to predict force.

3.3 Prediction Model

Different least-squares methods have been considered for use in analyzing the calibration data. Although a Total Least Squares approach might seem appropriate, since there is error in both the force sensor readings and the camera intensity data, the force sensors used in these experiments are so accurate (± 0.8mN) compared to the cameras that this method increases the prediction error. Currently, OLS is used to determine the model and Weighted Ordinary Least Squares (WLS) is used to validate the model and predict forces.

Since it would be undesirable to train the model to artifacts in the data, it is expected that many more images will be recorded than the minimum required to exactly determine all of the coefficients. In other words, $k \gg m \times n$, where $m \times n$ represents the resolution after the image has been registered and cropped. This ensures that the situation is more like curve fitting and less like polynomial interpolation.

To generate the model, the $\mathbf{A}$ matrix is partitioned as follows:

$$\mathbf{A} = \begin{bmatrix} \mathbf{a}^T \\ \mathbf{B}^T \end{bmatrix} \tag{6}$$

where

$$\mathbf{a} = \begin{bmatrix} a_1 \\ a_2 \\ \vdots \\ a_{mn} \end{bmatrix} \tag{7}$$

and

$$\mathbf{B} = \begin{bmatrix} b_1 & c_1 & d_1 \\ b_2 & c_2 & d_2 \\ \vdots & \vdots & \vdots \\ b_{mn} & c_{mn} & d_{mn} \end{bmatrix} \tag{8}$$

In addition to these two submatrices, the prediction model requires the covariance matrix of the calibration images $\boldsymbol{\Sigma} = \mathbf{cov}(\mathbf{P})$. This prediction model may then be expressed as $\mathbf{f} = \mathbf{C}\left(\mathbf{p} - \mathbf{a}\right)$, or:

$$\mathbf{f} = \left(\mathbf{B}^T \boldsymbol{\Sigma}^{-1} \mathbf{B}\right)^{-1} \boldsymbol{\Sigma}^{-1} \mathbf{B}^T \left(\mathbf{p} - \mathbf{a}\right) \tag{9}$$

This is recognizable as a weighted least squares solution to the equation $\mathbf{p} = \mathbf{B}\mathbf{f} + \mathbf{a}$ with weighting matrix $\boldsymbol{\Sigma}^{-1}$. The matrix $\mathbf{C} = \left(\mathbf{B}^T \boldsymbol{\Sigma}^{-1} \mathbf{B}\right)^{-1} \boldsymbol{\Sigma}^{-1} \mathbf{B}^T$ and the vector $\mathbf{a}$ are stored after calibration is completed for future use in force prediction.

4 Results

4.1 Model Validation

Verification of the model is achieved using a set of images collected using the procedure detailed in Section 2. The Measured Force $\mathbf{f}_m$ is stored at the time the images

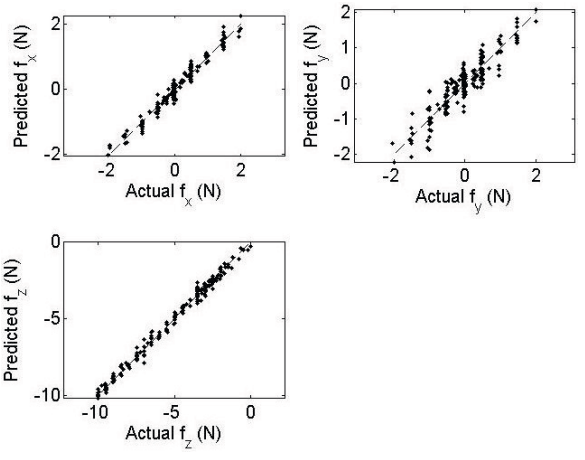

Fig. 8. Validation Error for Subject 5.

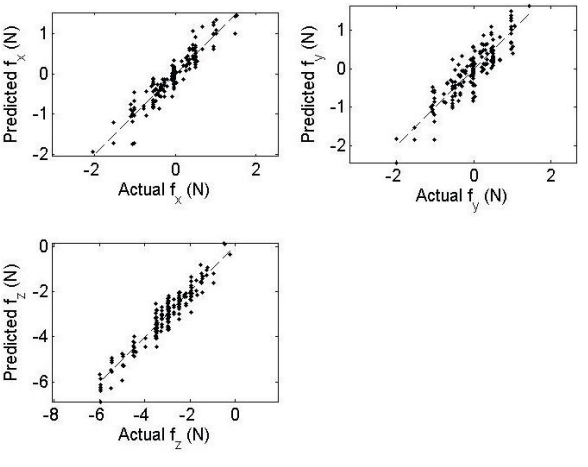

Fig. 9. Validation Error for Subject 6.

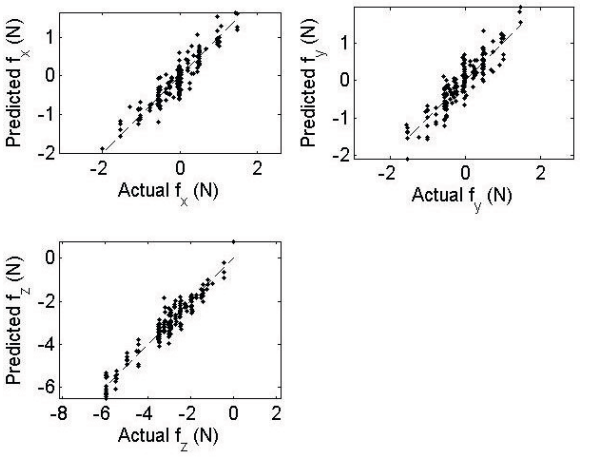

Fig. 10. Validation Error for Subject 7.

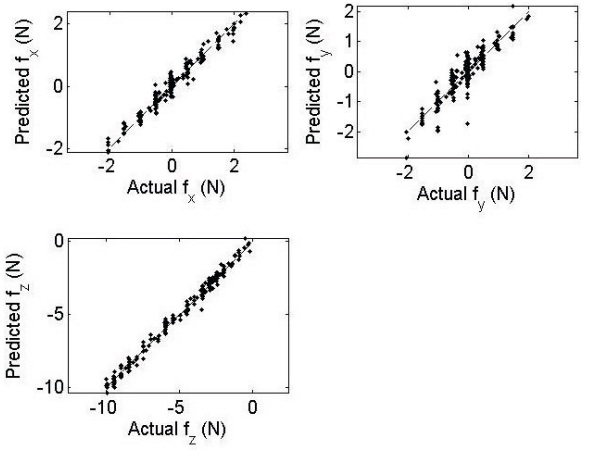

Fig. 11. Validation Error for Subject 8.

are collected. The images are registered using the procedure explained in Section 3.1. Equation 9 is used to obtain the Predicted Force $\mathbf{f}_P$ for each one. This force is compared to $\mathbf{f}_m$ and the RMS error in each direction for the set of images is determined. This error demonstrates the validity of the model in predicting forces when presented with new images. A plot of $\mathbf{f}_m$ vs. $\mathbf{f}_P$ for test subject 5 is shown in Figure 8. For this subject, 1300 calibration images were collected and another 200 validation images were set aside. The 1300 were used to form the model. In this case, the force was predicted on the validation images with an RMS error of 0.2 N in the x-direction, 0.3 N in the y-direction and 0.3 N in the z-direction.

The validation results for subject 6 are shown in Figure 9. For this subject, only 900 training images were collected for use in forming the model. Another 200 validation images were collected. The predicted force on these validation images had an RMS error of 0.2 N in the x-direction, 0.3 N in the y-direction and 0.4 N in the z-direction.

Subject 7's validation results are shown in Figure 10. 750 calibration images were recorded for this subject and 200 validation images tested the accuracy of the model. The RMS error of the validation image prediction was 0.2 N in the x-direction, 0.3 N in the y-direction and 0.4 N in the z-direction.

The validation results for subject 8 are shown in Figure 11. For this subject, 1200 calibration images were collected with 200 in the validation set. The x-, y- and z-direction RMS errors were 0.2 N, 0.3 N and 0.3 N, respectively.

In total, 20 individuals have been tested using this automated calibration routine. The validation results are similar to those described above. The average RMS error for shear force (x- and y-direction) is 0.3 N (which is 3% of the full range of ± 5 N). The average RMS error for normal force (z-direction) is 0.5 N (which is 5% of the full range of $0 - 10$ N).

5 Conclusions

This paper has shown a method of predicting force using fingernail imaging. The technique demonstrated is capable of predicting forces in three dimensions with RMS error less than 0.5 N. Future work includes the application of this method to human grasping exeriments. Success in this endeavor would allow grasping experiments to proceed without the need to instruct test subjects to precisely grasp objects exactly where the test object has been instrumented. Instead, a more natural grasp could be implemented, allowing the subject to comfortably position the hand in whatever manner desired. This would allow for the removal of one more potentially confounding variable in grasping studies, increasing their reliability.

Acknowledgements. This work was supported by NIH Grant 1R21EB004600-01A2 and IGERT Grant DGE-0654414.

References

1. Mascaro, S.A., Asada, H.H.: The common patterns of blood perfusion in the fingernail bed subject to fingertip touch force and finger posture. Haptics-e 4(3), 1–6 (2006)
2. Mascaro, S., Asada, H.: Photoplethysmograph Fingernail Sensors for Measuring Finger Forces without Haptic Obstruction. IEEE Trans. Robotics and Automation 17(5), 698–708 (2001)
3. Mascaro, S.A., Asada, H.H.: Measurement of Finger Posture and Three-Axis Fingertip Touch Force Using Fingernail Sensors. IEEE Trans. Robotics Automation 20, 26–35 (2004)
4. Sun, Y., Hollerbach, J.M., Mascaro, S.A.: Measuring fingertip forces by imaging the fingernail. In: 14th Symposium on Haptic Interfaces for Virtual Environment and Teleoperator Systems, pp. 125–131 (2006)
5. Sun, Y., Hollerbach, J.M., Mascaro, S.A.: Predicting fingertip forces by imaging coloration changes in the fingernail and surrounding skin. IEEE Trans. Biomedical Engineering 55(10), 2363–2371 (2008)

6. Sun, Y., Hollerbach, J., Mascaro, S.: Estimation of Finger Force Direction with Computer Vision. IEEE Trans. Robotics 25(6), 1356–1369 (2009)
7. Grieve, T., Lincoln, L., Sun, Y., Hollerbach, J.M., Mascaro, S.A.: 3D Force Prediction Using Fingernail Imaging with Automated Calibration. In: IEEE Haptics Symposium, pp. 113–120 (2010)
8. Berkelman, P., Hollis, R.: Lorentz magnetic levitation for haptic interaction: device design, function, and integration with simulated environments. Intl. J. Robotics Research 9, 644–667 (2000)
9. Sun, Y., Hollerbach, J., Mascaro, S.: Dynamic Features and Prediction Model for Imaging Fingernail to Measure Finger Forces. In: IEEE Intl. Conf. Robotics and Automation, pp. 2813–2818 (2006)